Th B2 08

The Next Generation Electromagnetic Acquisition System

A.K. Nguyen (Statoil ASA), P. Hanssen* (Statoil ASA), R. Mittet (EMGS AS), H.R. Jensen (EMGS AS), L.T.T. Fogelin (EMGS AS), M. Skarø (EMGS AS), M. Rosenquist (Shell International Exploration and Production), P. van der Sman (Shell Global Solutions Interna

Summary

We have compared field test data from a next generation node based CSEM acquisition system with data from a reference conventional system in a shallow water environment. The next generation system with much higher transmitter dipole moment and more sensitive receivers provides a step change improvement in the data quality, with clean data for all source frequencies out to 20 km offset compared to around 10 km offset for the reference system. The high data quality also provides clear improvements in the inversion results. This was demonstrated by improved imaging of a hydrocarbon accumulation under challenging conditions. We expect a maximal imaging depth, relative to the seabed, of up to 4500 m in future surveys with a commercial version of the next generation acquisition system.

Introduction

Since the first survey in Angola in 2000 (Eidesmo et al., 2002, Ellingsrud et al., 2002), the Controlled-Source Electro-Magnetic (CSEM) method (Cox 1980; Chave and Cox, 1982) has seen considerable development (Constable, 2010; Bhuiyan et al., 2013; Holten et al., 2014) and is now an established tool for hydrocarbon exploration.

The penetration depth is limited for marine CSEM. The reason for the limited penetration depth is the exponential decay with propagated distance for electromagnetic fields in conductive media. This exponential decay makes the electromagnetic signal insensitive towards deeply buried stratigraphy (Nguyen et al., 2016), including thin resistive layers, since the signals from these deep structures may be buried in the ambient noise. To overcome this limitation of the CSEM technology, EMGS, Shell and Statoil have executed a Joint-Industry Project (JIP) with the purpose of constructing a next generation acquisition system. The target was to increase the source dipole strength by a factor of 10 and also the receiver sensitivity by a factor of 10, measured from the 2011 state-of-the-art. With an increase of a factor of 100 in signal-to-noise ratio, the maximum imaging depth can be expected to increase by 2 km (Mittet and Morten, 2012). A prototype system with a new source and 10 receivers was completed in July 2016 and installed on the EMGS vessel Atlantic Guardian. Afterwards three successful field tests of the prototype system have been carried out. Here, we provide some details of this acquisition system together with the data and preliminary inversion results from one of the field tests.

Hardware improvements

The source system consists of a high voltage onboard power supply (24 kV) where the power is fed into the subsea power supply through an umbilical. The 1.5 MW subsea unit generates the waveform with amplitudes up to 10 kA to be transmitted by the horizontal electrical dipole solid antenna system. The subsea power supply is based on transistor inverter technology, and high precision in the transmitted source waveforms was demonstrated during the sea trials. The subsea source power supply is acoustically positioned from the vessel, and then the antenna is positioned relative to the subsea power supply using several position transponders on the antenna. To increase the position accuracy in deep water towing, the subsea source navigation system can position itself relative to a receiver when the transmitter is close to that receiver. This information can be used to correct the transmitter position for errors caused by the long distance between the vessel and the transmitter and hence increase the navigation accuracy.

The new receiver system (RxJ) is implemented with electrical field sensors designed to have a very low impedance to reduce the noise level. The magnetic field sensors are induction coils designed to have high sensitivity and low noise with respect to the size and weight. The positioning system of the receiver also includes a unit for acoustical measurement of the rotation of the sensor system. A precision built-in signal generator in the receiver system allows for advanced sensor calibration at the seabed to further increase the accuracy of the data. The receiver can do data processing for quality control purposes on the seabed, and transmit these data to the vessel. The RxJ units have a lower profile compared to the older Rx5 units to minimize motion and strumming noise.

Field test

Here we present some results from the first and smallest test, which consists of 11 Rx5 and 10 RxJ receivers, dropped along a south-north line and two inline towlines of 66 km each. Towline 1with the new prototype transmitter, had a dipole moment of 2.5×106 Am. This represents 70 percent of the dipole moment for the planned commercial version. Towline 2 has a lower dipole moment of 3.5×105 Am, the latter representing a conventional source dipole but with 10 percent higher dipole moment than the 2011 reference dipole moment. The test lines run over a producing field in the Norwegian Sea. This enables the verification of the inverted resistivity models against the current hydrocarbon-column model of the field. The water depth varies from 290 m to 350 m and the

reservoir depth is around 2600-2800 m below the sea surface with hydrocarbon accumulated in a stack of Jurassic sand layers. The field is heavily faulted with many compartmentalized segments and limited communication. Since the test field is in an area with relatively shallow water, has a large burial depth in terms of CSEM acquisition, 20 years of production and a significant amount of compartmentalized segments separated by some big faults, it is expected to be a challenging CSEM target.

Measured data

Figure 1 shows typical electric and magnetic data from the next generation system and the reference system for three different frequencies. Data for the next generation system comes from an RxJ receiver and the new transmitter. Data for the reference system comes from an adjacent Rx5 receiver and using the conventional transmitter dipole moment. The transmitter waveform has the power focused on the logarithmically spread frequencies 0.1, 0.2, 0.4, 0.8, 1.6 and 3.2 Hz.

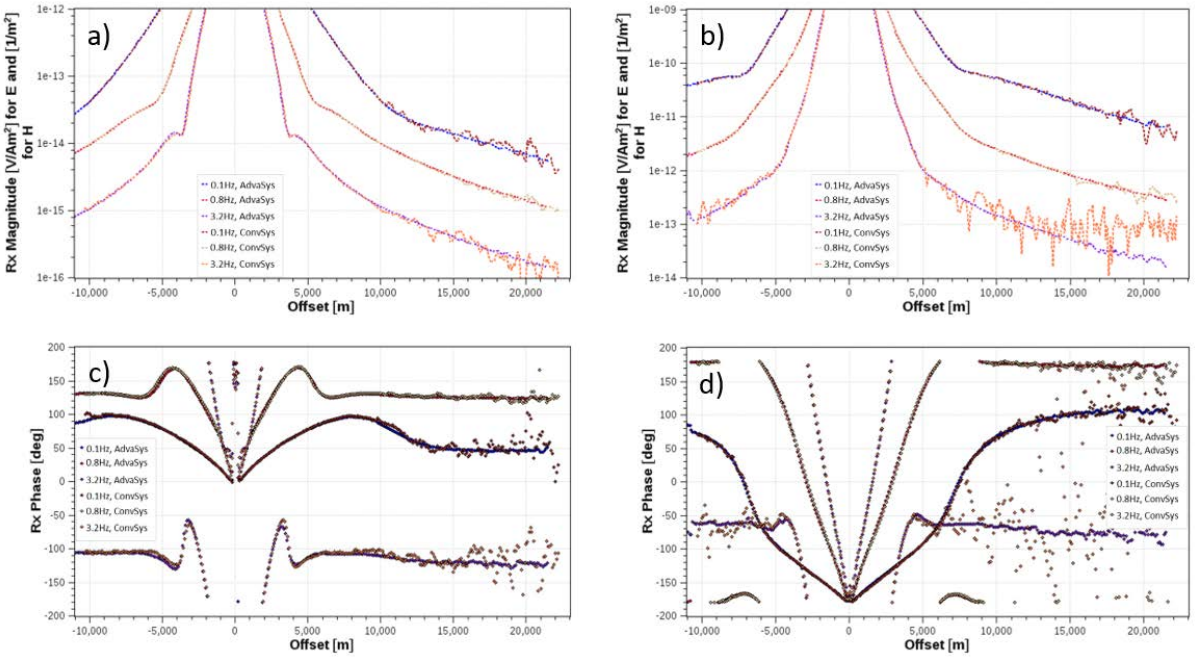

Figure 1 *Typical plots for inline electric field amplitude a) and phase c) versus offset for the advanced system and the conventional system, for three frequencies 0.1, 0.8, 3.2 Hz. Corresponding plots for the cross line magnetic field b) and d).*

We see in Figure 1a and 1c that the inline electric field amplitude and phase of the next generation system is clean and well behaved up to 20 km offset and beyond, while the corresponding electric field amplitude and phase for the reference dataset for 0.1 and 3.2 Hz start to become noisy around 10 km. The reason for the early noise entrance for 0.1 Hz is the swell noise in shallow water environments. The early noise entrance for 3.2 Hz is due to the increased damping for higher frequencies. The field from a lower amplitude transmitter simply disappears beneath the noise level at far offsets. We also see in Figure 1b and 1d that the magnetic amplitude and phase data for the next generation system are clean and well behaved out to 20 km for 0.1 and 0.8 Hz, and up to about 17 km for 3.2 Hz. For the reference system, the noise starts to enter already around 10 km for 0.1 and 0.8 Hz and the noise enters the magnetic data for 3.2 Hz already at 5 km offset.

The air-wave dominates the signal at large offsets, where the responses from the target are located. Figure 1 shows that this happens already at 4 km and 6 km for 0.8 and 3.2 Hz, respectively. The ability for the next generation system to acquire good data for both for the electric and magnetic field out to 20 km is thus very important for resistivity imaging of the deeper stratigraphy, since imaging

with shallow water techniques like up-down separation (Amundsen *et al.*, 2006; Mittet and Gabrielsen, 2013) requires low noise levels both for the electric and the magnetic data.

Inversion comparison

To show that the improvement in the data quality also provides improved resistivity imaging capability, we present here initial inversion results obtained by inverting data from the new prototype transmitter and from the reference transmitter. All receivers were included in the inversions. Data from the fourth receiver from the right was not recoverable leaving a small hole in the dataset. The blocky character of the fast-track inversion results in Figure 2 is a function of the coarse cell size and unrefined choice of regularization parameters. Although these are preliminary results, the inversions show the improvements from the new system, as described below.

To invert the measured inline electric field and crossline magnetic field, we used a pixel based, anisotropic 2.5D Gauss-Newton inversion (Hansen and Mittet, 2009). All frequencies: 0.1, 0.2, 0.4, 0.8, 1.6 and 3.2 Hz were used and up-down separation was applied in the inversion to attenuate the effect of the strong air wave. Maximum offset used was 16 km. The initial model is a simple water and formation model with formation resistivities of R_V=2.8 and R_H=2.2 Ωm. Vertical and horizontal smoothness regularization was used to stabilize the inversion. Both inversions used identical initial model and parameter settings and converged to a data misfit at 4 % in around 10 iterations.

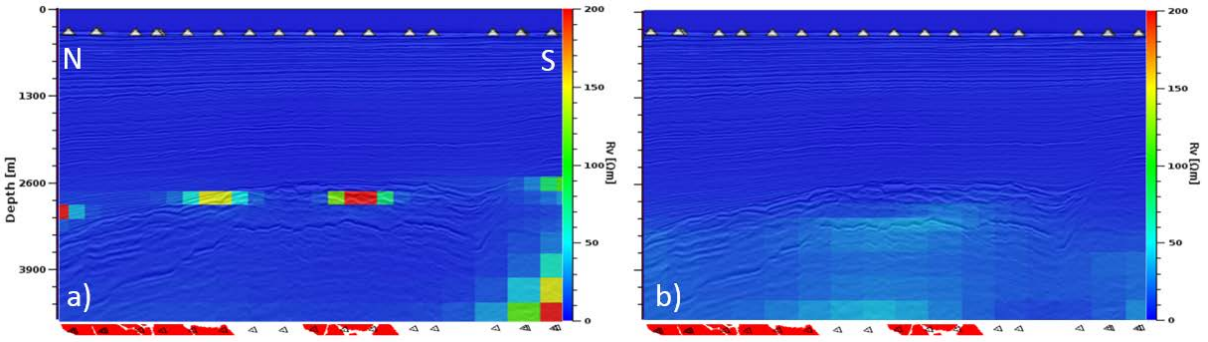

Figure 2: *Vertical resistivity obtained by inversion of data acquired with the new dipole (panel a) and old dipole (panel b). Red sections below both panels show the reservoir section with larger thickness right beneath the receiver locations.*

We see that the inverted vertical resistivity model of data from the new system (Figure 2a) shows two clear anomalies at reservoir level. A very strong anomaly is observed at the central, thick sand sections, no anomaly imaged across the big fault (receiver 8 and 9 from the right) where much of the reservoir sands have been eroded away and a weaker anomaly over the reservoir segments on the left hand side. There is no anomaly beneath the second and third receivers from the left, which confirms the poor reservoir properties of these drilled segments. Note that the resistivity anomalies are integrated results from the responses from all hydrocarbon filled sand layers. Figure 2b shows the inverted vertical resistivity model of data from the reference. Here only a faint anomaly over the whole field is reconstructed and placed slightly too deep. The weak responses from the deep buried hydrocarbon filled sand segments are most probably hampered by the ambient noise in the data.

Conclusions

We have compared field test data from a next generation node based CSEM acquisition system with data from a reference conventional system in a shallow water environment. The next generation system with much higher transmitter dipole moment and more sensitive receivers provides a step change improvement in the data quality, with clean data for all source frequencies out to 20 km offset compared to around 10 km offset for the reference system. The high data quality also provides clear improvements in the inversion results. This was demonstrated by improved imaging of a hydrocarbon

accumulation under challenging conditions. We expect a maximal imaging depth, relative to the seabed, of up to 4500 m in future surveys with a commercial version of the next generation acquisition system.

Acknowledgements

We thank Statoil, Shell and EMGS for the permission to publish this work. We also thank the License for permission to show the results and Arve Næss, Emmanuel Causse, Sebastian Ng and Mike Cogan for their support on various matters. The Next Generation Electromagnetic Equipment was partly funded by the Norwegian Research Council under the Demo 2000 program.

References

Amundsen, L., L. Løseth, R. Mittet, S. Ellingsrud, and B. Ursin [2006] Decomposition of electromagnetic fields into upgoing and downgoing components. Geophysics, **71**, G211–G223.

Bhuiyan, A., R. Sakariassen, Ø. Hallanger and A. McKay [2013] Modeling and interpretation of CSEM data from Bressay, Bentley and Kraken area of East Shetland Platform, North Sea. SEG Technical Program Expanded Abstracts: pp. 815-819.

Chave, A. D., and C. S. Cox [1982] Controlled electromagnetic sources for measuring electrical conductivity beneath the oceans: Part 1 - Forward problem and model study. Journal of Geophysical Research, **87**, B7 5327–5338.

Constable, S. [2010] Ten years of marine CSEM for hydrocarbon exploration. Geophysics, **75**, A67–A81.

Cox, C. [1980] Electromagnetic induction in the oceans and inferences on the constitution of the earth. Geophysical Surveys, **4**, 137–156.

Eidesmo, T., S. Ellingsrud, L. M. MacGregor, S. Constable, M. C. Sinha, S. Johansen, F. N. Kong, and H. Westerdahl [2002] Seabed Logging (SBL), a new method for remote and direct identification of hydrocarbon filled layers in deepwater areas using controlled source electromagnetic sounding. First Break, **20**, 144-152.

Ellingsrud, S., T. Eidesmo, S. Johansen, M.C. Sinha, L.M. MacGregor, and S. Constable [2002] Remote sensing of hydrocarbon layers by seabed logging SBL: Results from a cruise offshore Angola. The Leading Edge, **21**, 972–982.

Hansen, K. R. and R. Mittet [2009] Incorporating seismic horizons in inversion of CSEM data. SEG Technical Program Expanded Abstracts: pp. 694-698.

Holten, T., M. Commer, G. Newman, and S. L. Helwig [2014] 3D Inversion of Vertical Dipole - Time Domain CSEM data. EAGE Expanded Abstract.

Mittet, R. and J. P. Morten [2012] Detection and imaging sensitivity of the marine CSEM method. Geophysics, **77**, E411-E425.

Mittet, R. and P. T. Gabrielsen [2013] Decomposition in upgoing and downgoing fields and inversion of marine CSEM data. Geophysics, **78**, E1-E17.

Nguyen, A. K., J. I. Nordskag, T. Wiik, A. Kornberg Bjørke, L. Boman, O. M. Pedersen, J. Ribaudo, and R. Mittet [2016] Comparing large-scale 3D Gauss–Newton and BFGS CSEM inversions. SEG Technical Program Expanded Abstracts: pp. 872-877.